

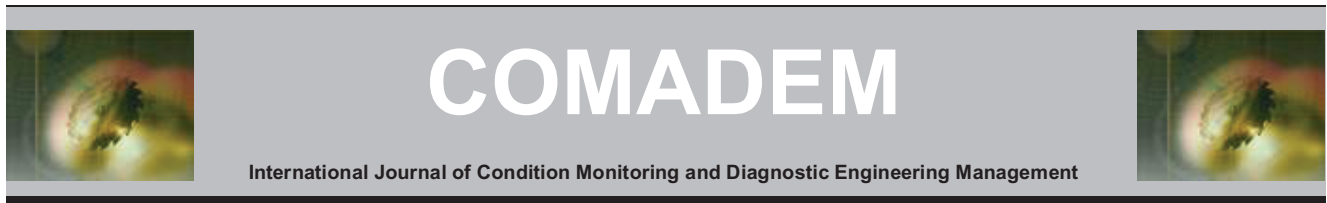
LIU, X., ZHU, G., ZHANG, Y., ASIM, T. and MISHRA, R. 2019. Performance improvement of a circulating fluidized bed boiler through flow modifications in primary air supply system. *International journal of condition monitoring and diagnostic engineering management* [online], 22(4), pages 29-43. Available from: <https://apscience.org/comadem/index.php/comadem/article/view/175>

Performance improvement of a circulating fluidized bed boiler through flow modifications in primary air supply system.

LIU, X., ZHU, G., ZHANG, Y., ASIM, T., MISHRA, R.

2019





Performance improvement of a Circulating Fluidized Bed Boiler through flow modifications in Primary Air Supply System

Xiaozhou Liu ^a, Guangyu Zhu ^a, Yu Zhang ^a, Taimoor Asim ^{b*} and Rakesh Mishra ^c

^a School of Material and Energy, Guangdong University of Technology, Guangzhou 510006, China

^b School of Engineering, Robert Gordon University, Aberdeen, UK (AB10 7GJ)

^c School of Computing & Engineering, University of Huddersfield, Huddersfield, UK (HD1 3DH)

* Corresponding author. Tel.: +44-1244-262457; email: t.asim@rgu.ac.uk

ABSTRACT

The primary air supply system is a key component of a Circulating Fluidized Bed (CFB) boiler. The uniformity of air flow through the primary air supply system is important for highly efficient operation of the CFB boiler. Non-uniform air flow distribution within the primary air supply system can affect the boiler's combustion adversely, resulting in higher energy consumptions. An effective measure to solve this problem is to install an air flow modifier in the primary air supply system. Thus, extensive numerical investigations have been carried out to design a suitable air flow modifier in order to improve operational efficiency of the CFB boiler. It has been shown that inhomogeneity in the air flow velocity, at a control cross-section of the wind-box, reduces from 65.79% to 21.25% when flow modifier is used. In order to validate the numerical results, visual and velocity distribution uniformity experiments have been conducted under five different test conditions. For this purpose, a small-scale model of a 220t/hr CFB boiler has been used. The experimental results substantiate the numerical predictions. Moreover, the same methodology has been implemented to a full-scale 220t/hr CFB boiler. The hot test results depict that the thermal efficiency of the boiler has increased from 85.71% to 88.34% when tested with an air flow modifier in place, which is equivalent to a saving of 5,000 tons of coal per year. The economic benefits of this energy-saving technology have been shown to be very significant, clearly demonstrating the effectiveness of the air flow modifier.

Keywords: Circulating Fluidized Bed (CFB); Computational Fluid Dynamics (CFD); Primary Air Supply System; Air Flow Modifier; Cold test; Error analysis

1. Introduction

Most Circulating Fluidized Bed (CFB) boilers, owing to their extensive fuel adaptability and low-cost pollution control, are widely used in power generation. The CFB boilers can easily handle combustion of inferior coal (calorific value of less than 4,000kcal). However, in recent years, numerous reports have pointed out that the thermal efficiency of CFB boilers is lower than expected. For example, Li [1] has reported that the exhaust flue gas temperature of a 220t/h CFB boiler can be as high as 168.5°C, with a thermal efficiency of 85.71%, which is lower than the expected design efficiency of 88%. This means that almost 5,000 tons of inferior coal is wasted every year. There are almost ten thousand CFB boilers currently in use in China alone. Hence, there is a strong demand to improve the thermal efficiency, and minimize the environmental impacts of the CFB boilers.

A CFB boiler utilizes a fluidized bed combustor in which crushed coal particles, smaller than 10mm in diameter, are suspended in a stream of upward flowing air. Combustion air is introduced into the combustion chamber through a set of nozzles installed on top of a wind-box. About 60% of the combustion air is passed through wind-box as primary air. Hence, the primary air supply system is one of the significant components of a CFB

boiler, comprising of a wind-box and an air-pipe. Wind-box is used to transport the primary air that mixes with crushed coal for efficient combustion in the boiler. Air is injected at a relatively high velocity through the air-pipe and into the wind-box. This results in non-uniform air flow distribution within the wind-box, leading to significant pressure non-uniformities. These air flow non-uniformities are associated with aerodynamic losses, resulting in inefficient combustion and high temperature of exhaust flue gas, along with a number of other problems [2]. Non-uniform air flow distribution within this component of the boiler thus leads to degradation in its thermal performance. In order to maintain stable and complete combustion, a large amount of air has to be injected into the wind-box of a CFB boiler as primary air. The oxygen content in the exhaust flue gas is as high as 9.13%. As a result, excess air ratio in the CFB boiler is significantly higher than normal. This generally leads to the high velocity of the air as high as 60m/sec at the outlet of air nozzles. A number of small carbon particles remain unburned and are carried out of combustion chamber by the flue gas, raising temperature of the exhaust flue gas significantly. Therefore, the thermal efficiency of the CFB boiler decreases. An effective measure to solve this problem is to install an air flow modifier in the wind-box of a CFB boiler. The purpose of the air flow modifier is to uniformly distribute the primary air into the fluidized bed, and hence, enhancing the combustion efficiency

considerably. In order to effectively design these flow modifiers for energy-saving purposes, extensive experimental and numerical investigations need to be carried out.

Numerous research studies on air distributors have been carried out by the researchers around the globe. For example, three-dimensional modelling of gas-solid flow in a fluidized bed combustion chamber, equipped with an inclined air distributor, has been carried out to explore the characteristics of the forces acting on a stagnant object at the bottom of the fluidized bed combustion chamber [3]. It has been found out that the distribution of the bubbles and particles are quite uneven at the bottom of the bed, due to the inclined air distributor. This leads to excessive circulation of the bubbles and particles. However, this inclined air distributor is installed at the bottom of the fluidized bed combustion chamber, and not in the wind-box [4]. Rahimpour et al [5] have studied the effect of distributor on fluidized bed's hydrodynamics. The pressure fluctuations have been measured in a fluidized bed of 0.15 m in diameter. The experiments have been carried out on three different types of distributors (i.e. perforated plate, bubble cap and porous plate) of different sizes and at various superficial gas velocities. It has been reported that the perforated plate distributor limits coalescence and lateral movement of bubbles. The distributors have been placed at the connection between the combustion chamber and the wind-box [6].

Luo et al [7] have studied heuristic shape optimization of a baffled fluid distributor for uniform flow distribution. A Computational Fluid Dynamics (CFD) based heuristic evolutionary algorithm has been developed for design optimization of baffled fluid distributor. Compared with the traditional arbitrary or empirical propositions, the optimization algorithm leads to an optimal baffle configuration for a given distributor geometry, which can be easily applied to different flow circuit geometries under different working conditions [8-11]. Wei et al [12] have investigated the design and optimization of baffled fluid distributor for realizing target flow distribution in a tubular solar receiver. It has been shown that the insertion of a geometrically optimized baffle is generally a practical solution for realizing non-uniform target distribution. Similar research studies have been carried out on the air flow in CFB boilers [13-14]. Lee et al [15] have studied the effects of primary to secondary air ratio on the performance of a commercial CFB boiler using a mathematical model. The calculated results are compared with the measured values from the CFB boiler. Mirek [16] has studied the primary air nozzles for large-scale CFB boilers using a combined numerical and experimental approach. As a result, a novel nozzle design has been developed whose geometry eliminates the majority of drawbacks typical of similar nozzles used in CFB boilers [17-19]. Bhasker [20] carried out numerical investigations on the air flow in the wind-box and developed a basic understanding for air flow distribution in it. Velocity vectors, flow lines, static pressure distributions and turbulence intensity patterns at different locations of the wind-box have been analysed. Moreover, numerical modelling techniques have been extensively used to model and analyse the complex flow behaviour in several industrial boilers [21-22].

Based on the detailed survey above, it is clear that the analyses regarding the effects of air flow distributing device in the wind-box of CFB boilers are severely limited. Air flow distribution uniformity in wind-box is an essential parameter that dictates the thermal efficiency of CFB boilers. Therefore, the numerical and experimental investigations of air flow distribution in CFB boiler wind-box are of great significance, and have been carried out in the present study. Based on the complex flow field

analyses within the wind-box of a CFB boiler, an air flow modifier has been designed, analysed and tested to evaluate its effectiveness.

2. Numerical Methodology

As mentioned earlier, the primary air supply system is one of the core systems of CFB boilers. Uniform air flow distribution in wind-box can result in higher overall thermal efficiency and smoke free combustion, as well as low energy consumption. Most of the coal-fired CFB boilers being used across the globe have a capacity of 220t/hr. Due to the sheer size of these boilers, and the exorbitant cost of carrying out experiments on them, it is prudent to use a scaled model of the boiler for both experimental and numerical investigations. Hence, a 1:64 scale model of the 220t/hr CFB boiler has been developed using a commercial CFD software Ansys 17.0 and has been termed as the baseline model hereafter. This section presents the details of the numerical modelling to analyse the flow behaviour within the CFB boiler.

2.1. Geometric modelling of the baseline boiler model

The primary air supply system of a CFB boiler comprises of a wind-box and an air-pipe. The air-pipe is located on one side of the wind-box, as shown in figure 1. The air enters the air-pipe through the air inlet, and then propagates to the wind-box and the combustion chamber. The bottom wall of the wind-box extends downwards obliquely by 10° . The height of the wind-box is $H_m=0.8\text{m}$, while its width is $W_m=0.84\text{m}$. It can be further seen in figure 1(b) that the depth of the wind-box is $L_m=1.8\text{m}$. Fifty cylindrical nozzles of 60mm in diameter are placed on the top wall of the wind-box. The geometric ratio of the baseline boiler model to the actual 220t/hr CFB boiler is 1:64.

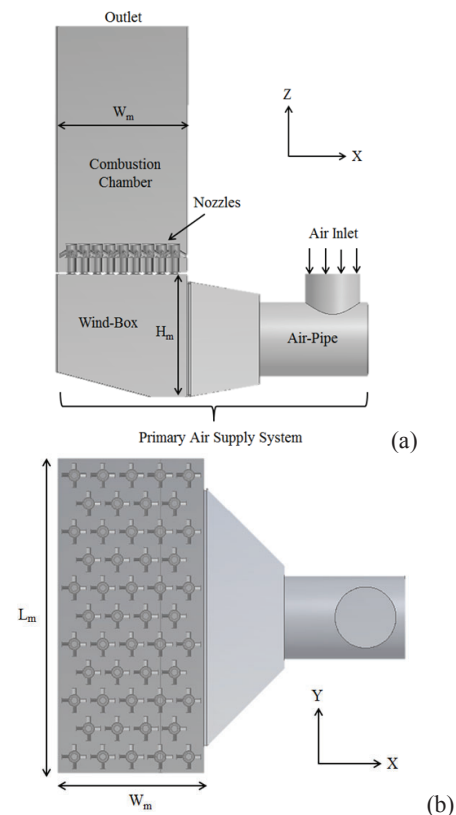


Figure 1. Geometrical model of the scaled CFB boiler (a) side view (b) top view

2.2. Spatial discretization and mesh independence

An unstructured tetrahedral mesh has been generated in the baseline boiler model for spatial discretisation of the flow domain. The size of the mesh around curves and in close proximity regions of the flow domain has been kept small enough to ensure accurate capturing of the complex flow phenomena. In order to obtain mesh independent results, six different mesh schemes with 7.6 million, 8.13 million, 8.66 million, 9.33 million and 10.04 million elements have been created for further analysis. For effective mesh independence analysis, a cross-sectional plane within the wind-box has been created at 0.85Hm (from bottom wall), named as plane P1. This plane has been chosen for analysis as it is near the nozzles yet maintains a reasonable distance from them so that the effects of the nozzles are not felt at this plane. For mesh independence analysis, three monitoring points (i.e. M11, M12 and M13) have been created on this plane, as shown in figure 2.

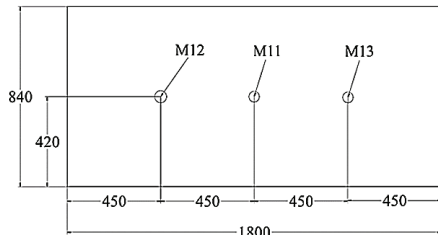


Figure 2. Schematic diagram of the cross-sectional plane P1 with monitoring points (dimensions are in mm)

The values of air flow velocity magnitude on cross-sectional plane P1, and on the monitoring points M11, M12 and M13, can be a good indicator for its role in normal fluidization and stable combustion within CFB boilers. Air flow velocity magnitude on the monitoring points has been recorded for the different mesh schemes considered in the present study (see table 1). It can be seen that as the number of mesh elements increases, the air flow velocity magnitude at all the monitoring points decreases. For example, increasing the number of mesh elements from 7.6 million to 8.13 million, the air flow velocity magnitude at points M11, M12 and M13 decreases by 6.9%, 5.9% and 4.3% respectively. It has been noticed that the difference in the air flow velocity magnitude reduces to below 3% when the number of mesh elements increases to 10.04 million. Therefore, it can be concluded that the mesh having 10.04 million elements is capable of accurately predicting the complex flow features, and hence is chosen for further analysis in the present study.

2.3. Selection of the physics models

Time averaged three-dimensional Navier-Stokes equations have been iteratively solved in a strong conservative form for the

steady flow of air within the CFB boiler model. A collocated variable arrangement is used to solve primitive variables (i.e. pressure and velocity components). The transport equations have been discretized using a conservative finite volume method [23-25]. Turbulence effects have been modelled using the standard two-equation k- ϵ turbulence model. It has been shown in numerous studies that the standard k- ϵ turbulence model is capable of predicting flow through ducts with reasonable accuracy [26-30]. A second order accurate skew upwind difference scheme, with physical advection correction scheme, has been employed to accurately compute the complex flow phenomena within the flow domain. A coupled algebraic multi-grid method solves this system of equations.

2.4. Boundary conditions and material properties

The inlet of the air-pipe has been modelled as velocity inlet at 20m/s while the outlet of the combustion chamber has been modelled as pressure outlet at 0Pa,g (atmospheric condition). All the walls in the flow domain have been modelled as stationary walls with no-slip condition. Isothermal flow of air enters the air-pipe at a constant density and dynamic viscosity of 1.225kg/m³ and 1.7895x10-5kg/m-s at 20°C respectively. The turbulent intensity and length scale of inlet air are of the order of 0.0245m and 3% respectively.

3. Verification of the numerical results

One of the most important steps while conducting numerical studies is the verification of the numerical results [30-33]. This means that some of the results obtained from the numerical simulations are compared with the experimental data in order to have confidence in the results obtained from these simulations [34-36]. For this purpose, three monitoring points have been chosen on the cross-sectional plane P1, which are different from the one mentioned earlier (i.e. M11, M12 and M13). This is because recording the data on these monitoring points is difficult to achieve experimentally. Hence, additional monitoring points M21, M22 and M23 have been created on plane P1 for verification purposes, as shown in figure 3.

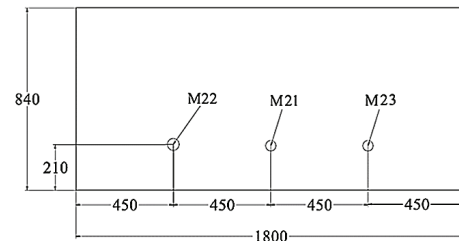


Figure 3. Monitoring points on the cross-sectional plane P1 (dimensions are in mm)

Table 1. Mesh independence results

Number of mesh elements (millions)	Velocity at M11 (m/s)	Velocity difference (%)	Velocity at M12 (m/s)	Velocity difference (%)	Velocity at M13 (m/s)	Velocity difference (%)
7.6	7.83		4.99		4.87	
8.13	7.32	6.9	4.72	5.9	4.67	4.3
8.66	7.11	4.3	4.53	4.2	4.51	3.5
9.33	6.95	3.8	4.40	2.8	4.36	3.3
10.04	6.79	2.0	4.31	2.1	4.27	2.1

Figure 4 depicts the values of z-velocity of air flow at the monitoring points M21, M22 and M23, from both CFD and experiments. It can be clearly seen that the CFD results are in close agreement with the experimental results, with an average variation of < 7%, indicating that the numerical modelling in the present study is reasonably accurate. Note: the details of the experimental setup will follow the section below on the discussions of numerical results.

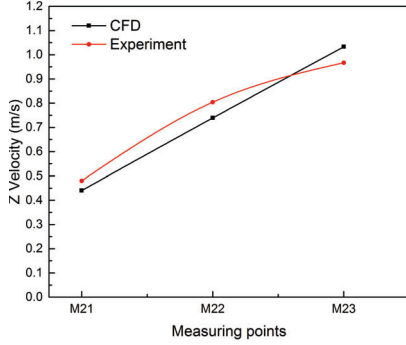


Figure 4. Verification of the numerical results

4. Discussions on the numerical results

Numerical modelling has significant cost advantages compared to field testing [37-40]. Numerical modelling provides additional insight into the complex flow phenomena using which, design changes can be suggested. Therefore, it is important to have a detailed discussion on the numerical results of the baseline boiler model to guide the design and operation of CFB boilers. The goal of the numerical simulations here is to improve the design of existing boiler components based on improved uniformity of air flow within the primary air supply system. In order to comprehensively analyse the uniformity of air flow in the wind-box, several cross-sectional planes have been created (i.e. P2, P3 and P4), in addition to plane P1, which are shown in figure 5.

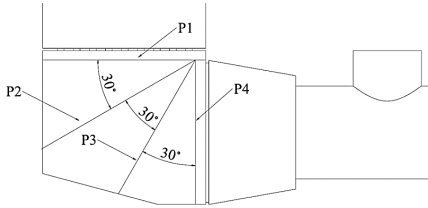


Figure 5. Schematic of cross-sectional planes P1, P2, P3 and P4

4.1. Flow behaviour within the baseline CFB boiler

The flow velocity distribution has been chosen as the primary flow parameter to analyse the uniformity of the air flow within the wind-box of the CFB boiler. Hence, figures 6 (a and b) depict the variations in air flow streamlines, coloured by flow velocity magnitude, on cross-sectional plane P1 (figure 6(a)) and in the flow domain (figure 6(b)) of the baseline boiler model. It can be clearly seen that there exist 2 large-scale vortical structures in the wind-box, just upstream the nozzles. The velocity gradient, as expected, is high in these structures. The highest flow velocity magnitude recorded on plane P1 is 12m/sec, while it reaches upto 86.9m/sec in the nozzles. Hence, the velocity of the flue gas particles in some regions of the combustion chamber is very high. A large number of carbon particles thus remain un-burnt and are carried out of the combustion chamber by flue gases,

raising the exhaust flue gas temperature significantly. This affects/reduces the thermal efficiency of the CFB boiler.

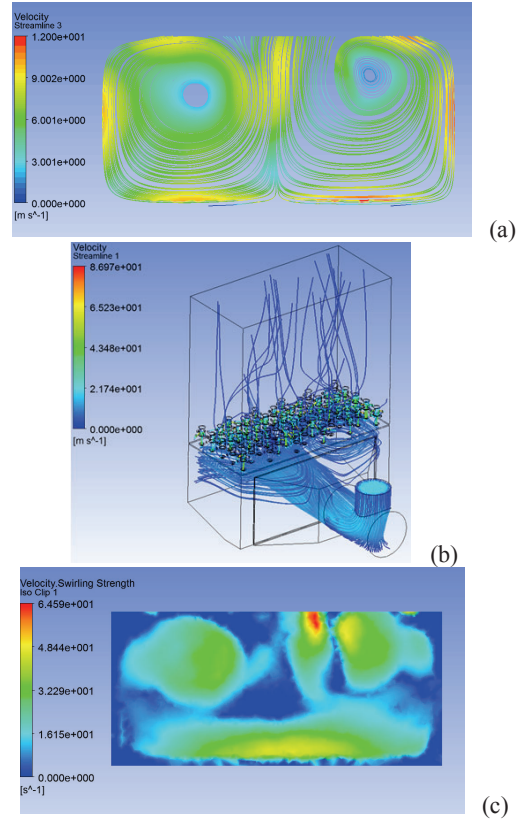


Figure 6. Flow distribution within the baseline boiler model (a) streamlines on plane P1 (b) streamlines in the flow domain (b) swirl strength on plane P1

Further analysing the flow non-uniformity within the wind-box of the baseline CFB boiler, the swirl strength parameter has been utilised here. The swirl strength (λ_{ci}) can be expressed as [23]:

$$\nabla u = [\bar{v}_r \ \bar{v}_{cr} \ \bar{v}_{ci}] \begin{bmatrix} \lambda_r & 0 & 0 \\ 0 & \lambda_{cr} & \lambda_{ci} \\ 0 & -\lambda_{ci} & \lambda_{cr} \end{bmatrix} [\bar{v}_r \ \bar{v}_{cr} \ \bar{v}_{ci}]^T \quad (1)$$

where λ_r is the real eigenvalue while λ_{ci} is the imaginary part of the eigenvalue of the velocity gradient tensor. The flow is considered to take place in the coordinate system spanned by $(\bar{v}_r, \bar{v}_{cr}$ and $\bar{v}_{ci})$, where the flow is stretched/compressed in \bar{v}_r direction, while it swirls in the plane spanned by \bar{v}_{cr} and \bar{v}_{ci} . The two distinct high-swirl regions are clearly visible in figure 6, which are the primary cause of air flow non-uniformity in the wind-box. The swirl strength on plane P1 can be seen to be as high as 64.6/sec, while the average swirl strength is around 16.7/sec.

Figure 7 depicts the average swirl strength on the cross-sectional planes P1, P2, P3 and P4, as shown in figure 5. The flow in the wind-box is from plane P4 to plane P1. It can be seen in figure 7 that at the entrance of the wind-box, the average swirl strength is low (about 8.9/sec on plane P4), while it significantly increases downstream. At plane P3, the average swirl strength increases by 85%. This is because of the non-uniformity of air flow once it enters the wind-box, and its direction changes.

Furthermore, from planes P3 to plane P2, the average swirl strength of the flow decreases by 12.1% due to straightening of air flow streamlines. From planes P2 to P1, the average swirl strength has been observed to increase by 15.1%. On average, the swirl strength in the wind-box is 14.1, which is very high, and is representative of considerable air flow non-uniformity within it.

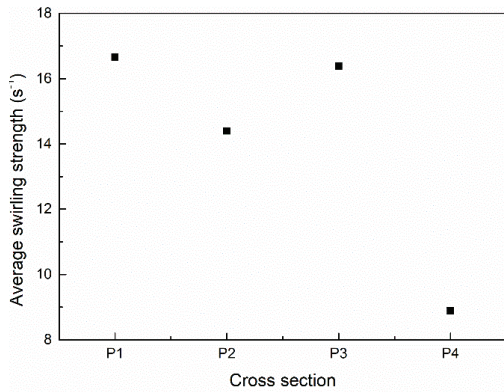


Figure 7. Average swirl strength variations along the cross-sectional planes P1, P2, P3 and P4 of the baseline CFB boiler model

It is clear from these discussions that the current CFD boiler design needs to be modified in order to reduce air flow non-uniformity within the combustion chamber of the CFB boiler.

4.2. Flow behaviour within the CFB boiler having a perforated plate

A perforated plate is an effective measure to achieve uniformity in the flow field [11]. Thus, a perforated plate has been installed at the interface between the wind-box and the air-pipe in order to evenly distribute the incoming air. The details of the perforated plate used are shown in figure 8. It can be seen that the perforated plate comprises of 162 square channels.

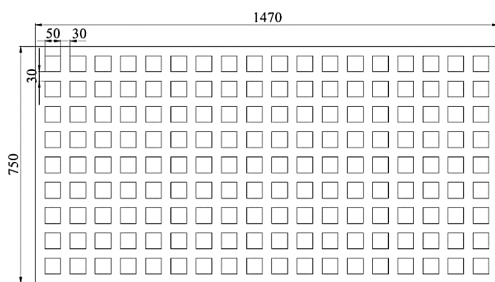


Figure 8. Schematic of the perforated plate (dimensions in mm)

Figure 9 depicts the flow behaviour within the CFB boiler with the perforated plate installed at the entry of the wind-box. Figures 9(a and b) shows the variations in air flow streamlines on the cross-sectional plane P1 (figure 9(a)) and in the flow domain (figure 9(b)) of the perforated plate boiler model. It can be clearly seen in comparison with the flow behaviour in the baseline boiler model that the flow is more uniformly distributed within the wind-box of the boiler. The large vortical structures observed in the case of the baseline boiler model have been disintegrated into much smaller areas of recirculation, thereby reducing the maximum air flow velocity magnitude by 63.4% on cross-sectional plane P1, and by 9.8% within the nozzles. Lower flow velocities result in more efficient combustion, reducing the energy losses within the boiler.

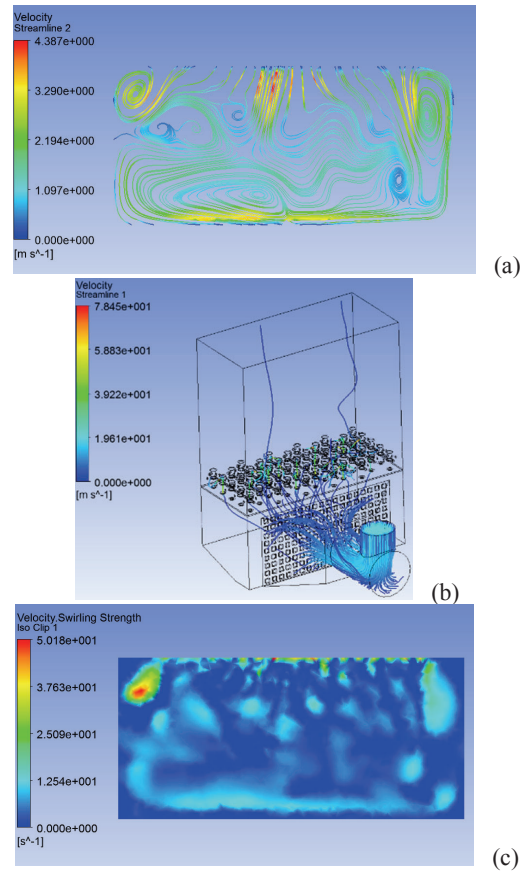


Figure 9. Flow distribution within the boiler model with a perforated plate (a) streamlines on plane P1 (b) streamlines in the flow domain (c) swirl strength on plane P1

It can be further seen in figure 9(c) that the maximum and average swirl strength on plane P1 has decreased by 22.3% and 70.8% respectively, in comparison with the baseline boiler model. Although there is still some regions of localised high swirl strength on plane P1, in comparison with figure 6(c), the swirl strength has decreased significantly just before the nozzles, indicating increased air flow uniformity.

Figure 10 draws a comparison of the average swirl strength on the various planes within the wind-box (shown in figure 5), between the perforated plate and the baseline CFB boiler models. On plane P4 (i.e. at the entry of the wind-box), the average swirl strength in the perforated plate model has increased by 32.5% in comparison with the baseline boiler model. This is because of the jet action caused by the air flow channels in the perforated plate. On planes P3, P2 and P1 (i.e. along the wind-box), the average swirl strength in the perforated plate model decreases by 55%, 49% and 71% respectively, in comparison with the baseline boiler model. Similarly, the average swirl strength in the entire wind-box decreases by 43.9%. This clearly shows that air flow in the perforated plate CFB boiler is substantially more uniform than the baseline boiler. As a result, the thermal efficiency of the CFB boiler is expected to improve.

Although the installation of a perforated plate at the entry of the wind-box has proved to be very useful in achieving air flow uniformity within the CFB boiler, however, published literature also suggests that using baffles is another effective measure that can be taken in this regard [7]. Hence, in the present study, a combination of techniques have been analysed in order to achieve maximum air flow uniformity in the CFB boiler.

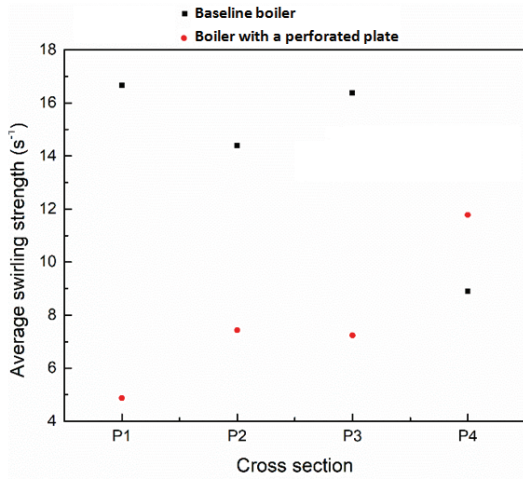


Figure 10. Comparison of the average values of swirl strength between the baseline and perforated plate models of the CFB boiler

4.3. Flow behaviour within the perforated plate CFB boiler having a baffle

In the early design phase, this study investigates the usefulness of a single baffle plate being installed on in the wind-box. As shown in figure 11, the angle between the baffle and the bottom wall (straight section) of the wind-box is fixed at 30°. This is in accordance with the requirements of the persons of special equipment institute, for the convenience of maintenance. The baffle is installed at a distance of 0.2W_m from the perforated plate, and has a length of 0.2H_m.

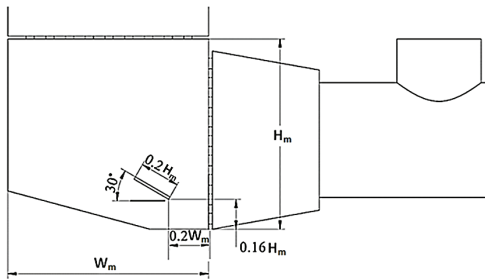


Figure 11. Schematic of the baffle

Figure 12 shows the variations in the flow field within the CFB boiler model installed with a baffle in the wind-box. It can be seen in figures 12 that although the air flow velocity magnitude within the wind-box remains almost the same as in case of a perforated plate CFB boiler model, the maximum and average swirl strength of air flow on cross-sectional plane P1 has decreased by 12.9% and 0.6% respectively. The velocity magnitude coloured flow streamlines are more uniformly distributed on plane P1 (figure 12(a)), although there are still some regions of flow recirculation. Moreover, the concentration of high swirl strength regions is more diffused than the perforated plate model. Hence, it can be concluded that the addition of a baffle enhances the uniformity of air flow within the combustion chamber of a CFB boiler by decreasing the swirl strength, while keeping the air flow velocity almost the same.

Figure 13 shows the comparison of the average swirl strength on cross-sectional planes P1 to P4, between the baseline, a perforated plate and perforated plate with a baffle CFB boiler

models. On plane P4, the average swirl strength in the model with a baffle has decreased by 5.9% in comparison with the perforated plate model. However, on other planes (i.e. P3, P2 and P1), the average swirl strength remains almost the same as observed in case of the perforated plate model. Hence, the effect of using a single baffle is more prominent at the entrance of the wind-box, making air flow more uniformly distributed. On average, the swirl strength in the wind-box of the boiler model with a baffle decreases by 1.3% as compared to the perforated plate model.

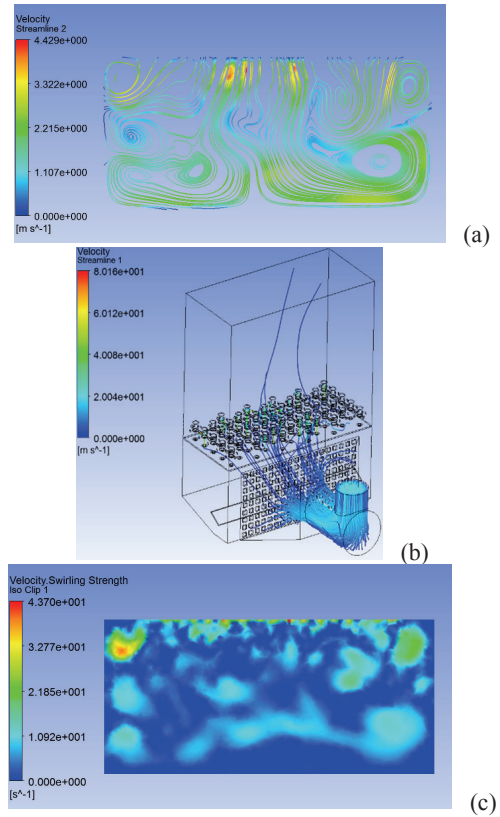


Figure 12. Flow distribution within the boiler model with a baffle (a) streamlines on plane P1 (b) streamlines in the flow domain (c) swirl strength on plane P1

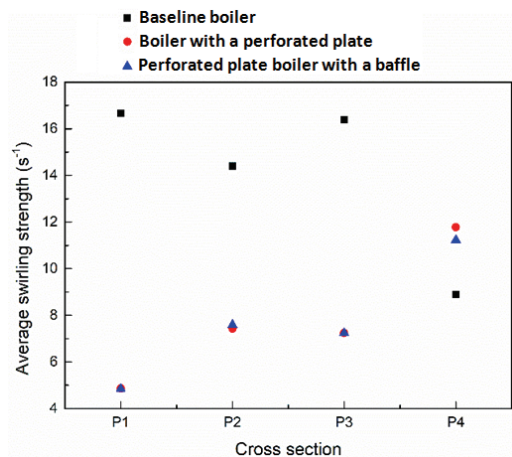


Figure 13. Comparison of the average swirl strength between the baseline, a perforated plate and single baffle models of the CFB boiler

4.4. Flow behaviour within the perforated plate CFB boiler having two baffles

In the second stage of investigating the effects of baffles on air flow uniformity within the combustion chamber of a CFB boiler, an additional baffle has been installed within the wind-box, downstream the first baffle discussed earlier. The length of the second baffle is the same as the first one, while its angle from the horizontal axis has been increased to 60° in order to direct air flow towards the nozzle in a more streamlined manner. Figure 14 shows the schematic of the two baffles model. The second baffle has been placed horizontally at 0.6W_m.

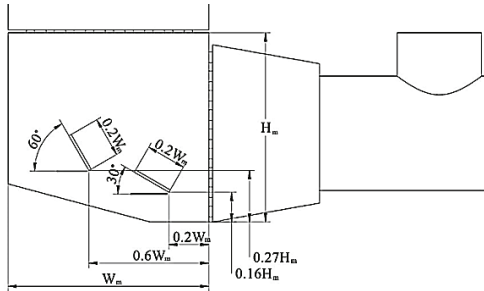


Figure 14. Schematic of two baffles model

Analysing the flow behaviour and its uniformity in the wind-box of the CFB boiler, air flow streamlines, coloured by flow velocity magnitude, have been drawn in figures 15(a and b). In comparison with figure 12, it can be seen that the maximum flow velocity magnitude over the cross-sectional plane P1 has decreased by 6.1%, compared to the boiler model with a single baffle. The flow velocity within the nozzles and the swirl strength on plane P1 remains almost the same; however, the strength of the swirling motion is more diffused in the flow domain. Hence, the introduction of a second baffle in the CFB boiler decreases the flow velocity upstream the nozzles, thereby helping in the combustion process by allowing ample time for the carbon particles to burn. This also keeps in the check the quality of flue gases, and hence, the thermal efficiency of the boiler is improved.

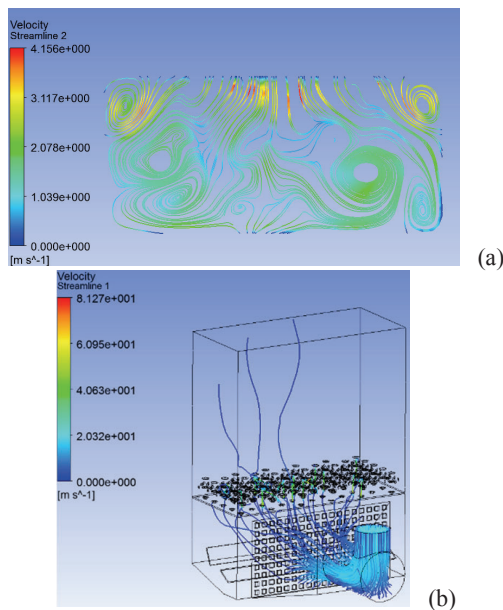


Figure 15. Flow distribution within the boiler model with two baffles (a) streamlines on plane P1 (b) streamlines in the flow domain (b) swirl strength on plane P1

Analysing the average swirl strength in different sections of the wind-box, it can be seen in figure 16 that there is insignificant improvement/decrease in the swirl strength when two baffles are used. This statement is in-line with the above discussions i.e. the second baffle has more profound effect on the flow velocity, rather than the swirl strength. Anyhow, a reduction of 1.9% in the swirl strength at cross-sectional plane P2 has been recorded, in comparison with a single baffle boiler model. The reason for this slight decrease in the swirl strength is the fact that the second baffle is installed just upstream plane P2. Thus, the streamlining of air flow caused by the deviation from the second baffle decreases the swirling motion in that region. The average reduction in the swirl strength, in the wind-box, has been computed to be 0.4%.

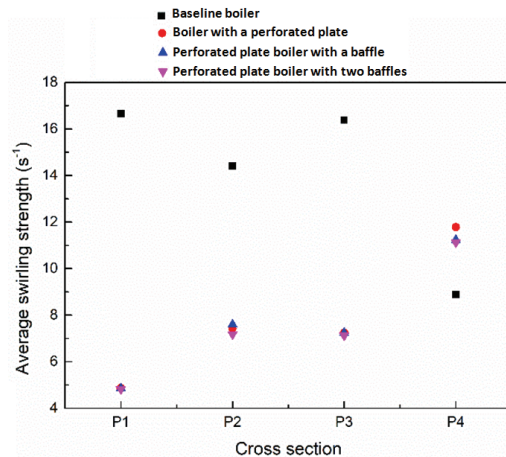


Figure 16. Comparison of the average values of swirl strength between the baseline, a perforated plate, single and two baffle models of the CFB boiler

4.5. Flow behaviour within the perforated plate CFB boiler having three baffles

In the third and final stage of investigating the effects of baffles on air flow uniformity within the combustion chamber of a CFB boiler, a third baffle has been installed at a strategic location within the wind-box. It has been in the case of two baffles model that some air particles, after striking the first baffle, are reflected to such an extent that they never reach the second baffle. Thus, a third baffle has been installed at an angle of 60° with the horizontal axis, just downstream the first baffle, and following the streamlines of air flow observed earlier. It is expected that this arrangement of baffles will engage most of the air particles entering the wind-box, and will aid in enhancing the thermal efficiency of the CFB boiler by making the flow more uniform. The schematic of three baffles boiler model is shown in figure 17. It can be seen that the length of all the baffles has been kept

the same. The third baffle has been placed in-between the first and the second baffles horizontally i.e. at $0.4W_m$.

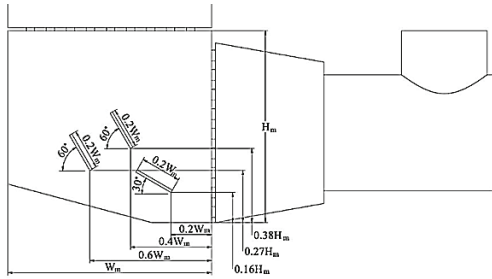


Figure 17. Schematic of three baffles model

Figure 18 depicts the flow velocity magnitude and swirl strength variations within the CFB boiler model installed with a perforated plate and three baffles. In comparison with figure 15(a), it can be clearly seen in figure 18(a) that the flow has become more uniform. The areas of flow recirculation observed in case of two baffles model is now restricted to far ends of cross-sectional plane P1. The localised flow velocity magnitude has although increased slightly, the average flow velocity has decreased. It can be further seen in figure 18(b) that the air particles that were unable to contact the second baffle, are now being deflected by the third baffle, thereby making air flow more uniform in the wind-box of the boiler. The average swirl strength on the cross-sectional plane P1, as shown in figure 18(c), has decreased by 7.4% in the three baffles model, compared to two baffles models.

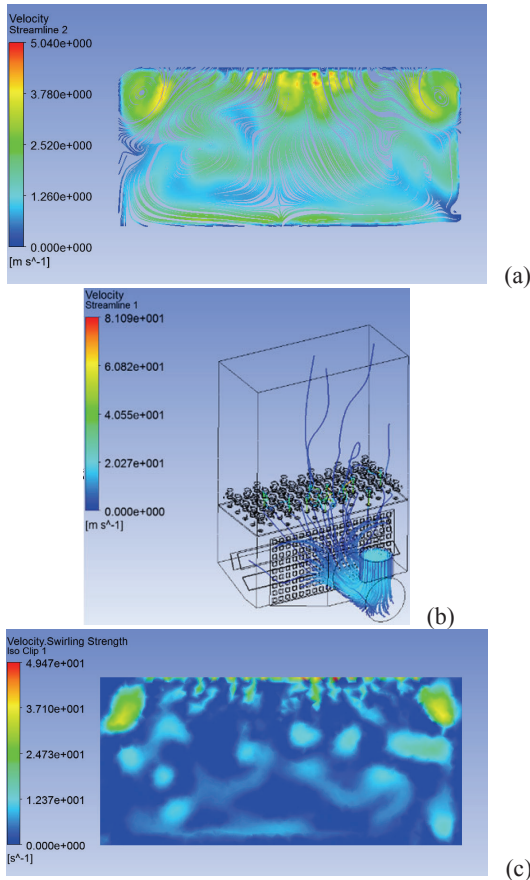


Figure 18. Flow distribution within the boiler model with two baffles (a) streamlines on plane P1 (b) streamlines in the flow domain (c) swirl strength on plane P1

A comprehensive comparison of average swirl strength on the different planes considered here is presented in figure 19. In comparison with all the different boiler configurations discussion above, for the first time now, the average swirl strength keeps on decreasing from the entrance to the exit of the wind-box i.e. average swirl strength on P2 is less than on P1. This is a clear indication of appropriate flow streamlining in the combustion chamber of the CFD boiler, which is expected to result in expected burning of carbon particles, thereby enhancing the thermal efficiency of the boiler. It has been enumerated that, in comparison with two baffles model, in three baffles model, the average swirl strength on cross-sectional plane P4 to P1 decreases by 10.2%, 19.4%, 16.9% and 7.4% respectively.

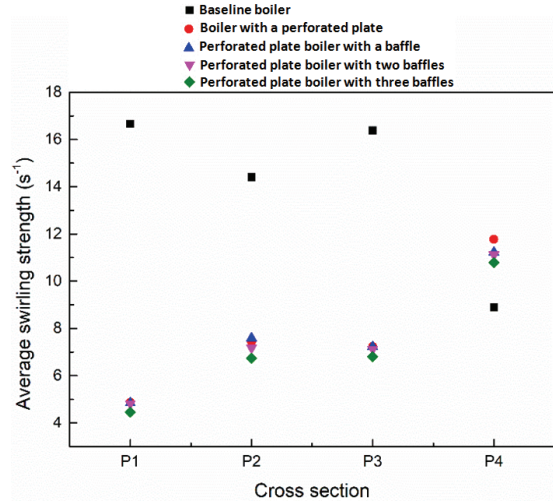


Figure 19. Comparison of the average values of swirl strength between the baseline, a perforated plate, single, two and three baffle models of the CFB boiler

A maximum number of three baffles is deemed appropriate/practical due to the limited space in the wind-box of the boiler, and because more number of baffles become inconvenient for the workers to install and maintain. Thus, the flow modifier comprising of a perforated plate and three baffles is considered as the best choice in the current scenario.

5. Design optimisation of the flow modifier

Design optimisation of the air flow modifier is essential in order to maximise the benefits it provides. There are various design optimisation techniques available in the literature. The one considered here is based on systematic parametric investigation of the orientation and geometrical dimensions of the three baffles used in the flow modifier. The numerical simulations required to carry out the design optimisation of the flow modifier have been identified based on Design of Experiments (DoE) [41-42]. In DoE based studies, the first step is the identification of key dimensions that need to be investigated. In the case of the air flow modifier considered in the present study, these dimensions (or factors) are:

1. Angle of baffles 2 and 3 with respect to the horizontal (Factor A)
2. Horizontal distance between the perforated plate and the 1st baffle (Factor B)
3. Length of all the baffles (Factor C)

4. Vertical distance between the bottom wall of the wind-box and the 1st baffle (Factor D)
- 5.

These factors are schematically shown in figure 20. It can be seen that the horizontal distance between baffles 1 and 3, and between baffles 3 and 2, has been kept constant at $0.2W_m$. Similarly, the vertical distance between baffles 1 and 2, and between baffles 2 and 3, has been kept constant at $0.1H_m$. As discussed earlier, the angle of the first baffle is fixed at 30° due to convenience of maintenance etc.

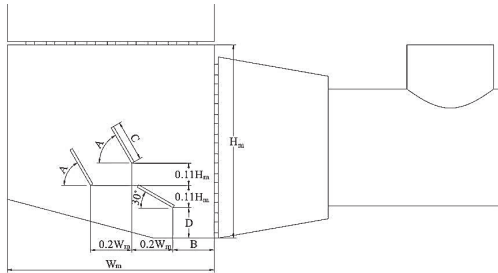


Figure 20. Factors considered in the Design of Experiments

There are certain constraints to these factors as well. For the convenience of maintenance, the angles that baffles 2 and 3 make with the horizontal cannot be greater than 60° . Hence, three levels of factor A are considered. These levels are 30° , 45° and 60° with respect to the horizontal. Similarly, there are three levels considered for factors B, C and D as well. Table 2 summarises the levels considered for each factor. It can be seen that the horizontal distances considered between the perforated plate and the first baffle are $0.1W_m$, $0.2W_m$ and $0.3W_m$ respectively. The lengths of the baffles considered are $0.1W_m$, $0.15W_m$ and $0.2W_m$ respectively. The three levels considered for factor D are $0.16H_m$, $0.27H_m$ and $0.38H_m$.

A four-factor, three-level orthogonal matrix (shown in table 2) is obtained by selecting the L9 (34) orthogonal array. In total, nine geometrical configurations have been identified that need to be investigated. Each row of table 2 represents a numerical simulation that needs to be performed.

Table 2. Orthogonal experimental table L9 (34)

Geometric Configuration	Levels of Factor A ($^\circ$)	Levels of Factor B (W_m)	Levels of Factor C (W_m)	Levels of Factor D (H_m)
1	30	0.1	0.1	0.16
2	30	0.2	0.15	0.27
3	30	0.3	0.2	0.38
4	45	0.1	0.15	0.38
5	45	0.2	0.2	0.16
6	45	0.3	0.1	0.27
7	60	0.1	0.2	0.27
8	60	0.2	0.1	0.38
9	60	0.3	0.15	0.16

As discussed earlier, the primary purpose of air flow modifier is to achieve more uniform flow within the wind-box of the CFB boiler. The aforementioned analysis has shown that swirl strength is a useful flow based parameter that evaluates flow uniformity. Thus, average swirl strength has been computed numerically on the cross-sectional planes already discussed i.e. planes P1, P2, P3 and P4. The variations in the average swirl strength, for the geometrical configurations/conditions identified in table 2, have been plotted in figure 21. It can be seen that the average swirl strength in case of three baffles keeps on decreasing from the

entrance (P4) to the exit (P1) of the wind-box, which is in-line with earlier observations. It can be further noticed that condition 5 results in minimum swirl strength. Condition 5 corresponds to $A=45^\circ$, $B=0.2W_m$, $C=0.2W_m$ and $D=0.16H_m$, and is the optimal air flow modifier design.

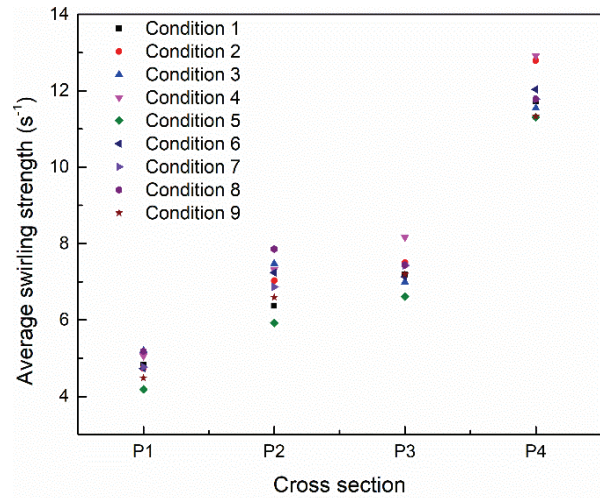
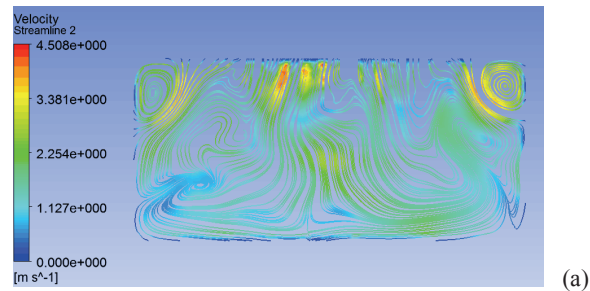


Figure 21. Comparison of the average values of swirl strength between the different geometrical conditions identified, at cross-sectional planes P1, P2, P3 and P4

After the identification of the optimal flow modifier design, its performance needs to be evaluated and compared against the 3 baffles models discussed in section 4.5. For this purpose, air flow streamlines on cross-sectional plane P1, and in the whole flow domain are shown in figures 22(a and b), while the local swirl strength variations on plane P1 are shown in figure 22(c). In comparison with figure 18, it can be seen that the maximum air flow velocity on plane P1 has decreased by 10.5%. The air flow on plane P1 is quite evenly distributed, while the air flow exiting from the nozzles is more uniform than in the 3 baffles model. The average swirl strength on plane P1 has been recorded to be the same as in case of 3 baffles model. Hence, it can be concluded that the optimally designed air flow modifier depicts lower flow velocity than the 3 baffles model, thereby enhancing the thermal efficiency of the CFB boiler by offering more uniform combustion.



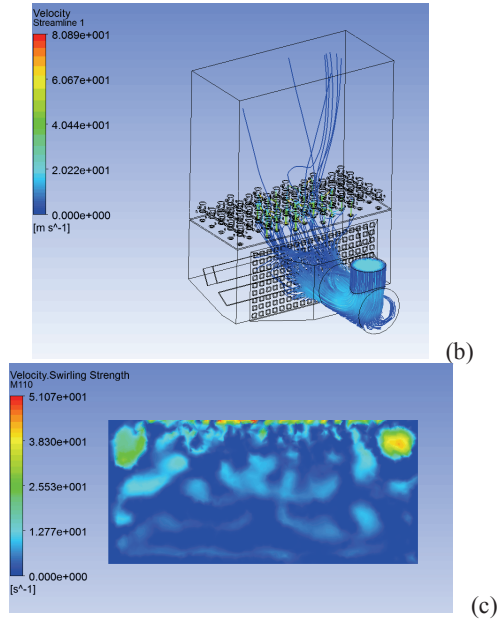


Figure 22. Flow distribution within the optimised boiler design (a) streamlines on plane P1 (b) streamlines in the flow domain (b) swirl strength on plane P1

Further analysing air flow behaviour within the wind-box of the CFB boiler, installed with optimally designed air flow modifier, figure 23 depicts a comparison of z component of flow velocity on cross-sectional plane P1. Figure 23(a) corresponds to the CFB boiler model with no air flow modifier installed, while figure 23(b) corresponds to the CFB boiler installed with optimally designed air flow modifier. It can be clearly seen that the flow velocity decreases significantly once the air flow modifier is installed. This helps in more uniform flow distribution within the wind-box of the boiler, leading to normal fluidization, stable combustion and safe operation of the CFB boiler.

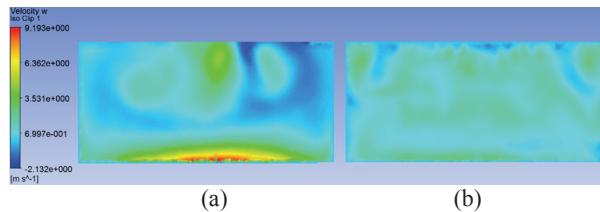


Figure 23. Variations in Z component of air flow velocity at plane P1 (a) without the air flow modifier (b) with the air flow modifier

In order to evaluate the effectiveness of the optimally designed air flow modifier, inhomogeneity in the z component of flow velocity, at cross-sectional plane P1, has been used. The flow velocity inhomogeneity can be expressed as [43]:

$$\xi = \sqrt{\frac{1}{n} \sum_{i=1}^n \left(\frac{u_i - \bar{u}}{\bar{u}} \right)^2} \times 100 (\%) \quad (2)$$

where ξ is the flow velocity inhomogeneity, u_i is the local flow velocity in z direction at plane P1, \bar{u} is average flow velocity in z direction at P1 and n are the number of measurement points in plane P1. Flow velocity inhomogeneity on plane P1, in case of the CFB boiler without the air flow modifier, has been computed to be $\xi_1=81\%$, while it is $\xi_2=24\%$ for the boiler model installed with optimally designed air flow modifier. Thus, it can be inferred that flow velocity homogeneity significantly increases as

an air flow modifier is installed in a CFB boiler. The effectiveness of air flow modifier is reflected by flow velocity inhomogeneity reduction on the plane P1, which can be expressed as:

$$\Delta\xi = \frac{(\xi_1 - \xi_2)}{\xi_1} \quad (3)$$

where $\Delta\xi$ is the percentage reduction in flow velocity inhomogeneity. $\Delta\xi$ for figure 23 has been computed to be $(81-24)/81=70\%$. This means that the optimally designed air flow modifier is 70% effective in uniformly distributing air flow within the wind-box of the CFB boiler. The next step is to experimentally prove that the optimal air flow modifier designed here actually improves air flow distribution within a CFB boiler.

6. Cold testing of the optimal boiler model

In order to ascertain the correctness of the numerical results obtained in the previous section regarding the optimal CFB boiler model, cold tests have been carried out using a small size model (the same dimensions as in the numerical model). Figure 24 shows the test boiler facility and its schematic. The test facility comprises of an air supply system and an air distribution system. The air supply system is composed of a centrifugal fan and an air supply pipe, while the air distribution system is composed of a wind-box and the flow modifier. The flow-modifier further comprises of a perforated plate and three baffles. Fifty wind caps (nozzles) installed on the top wall of the wind-box provide the primary air to the combustion chamber. The combustion chamber is made of Plexiglas and steel.

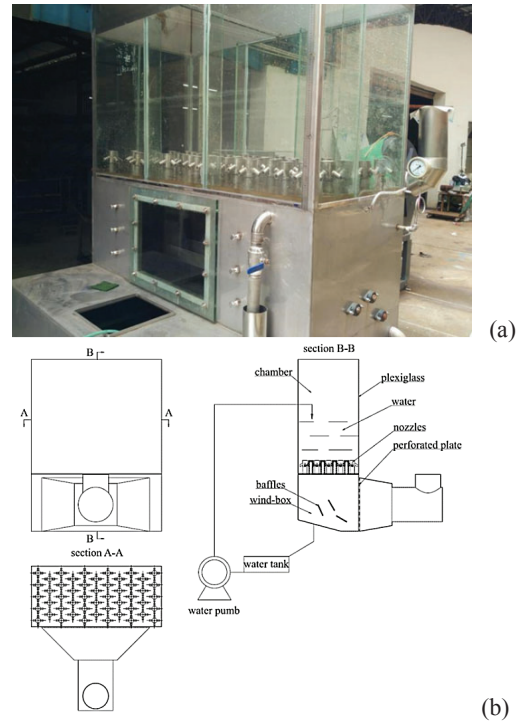


Figure 24. Optimised boiler (a) test facility (b) schematic of the facility

The cold tests have been carried out on five different test conditions, as summarised in table 3. It can be seen that various fan's operating frequencies, ranging between 10.7Hz and 50Hz, have been considered that deliver a range of air flow volumes, and hence, air flow velocities. Air flow velocity in z-direction (towards the nozzles and combustion chamber) has been

measured on the monitoring points M21, M22 and M23, as shown and discussed in figure 3, using a hot wire anemometer, which has an accuracy of 0.01m/sec.

Careful visual inspections and extensive data analysis on air flow velocity has been carried out in the present study to quantify the effectiveness of flow modifier for air flow uniformity in the wind-box of the optimised CFB boiler model. The operational procedure followed during the cold tests can be outlined as:

1. The combustion chamber is filled with water by using a water pump, until the water level reaches 600mm in the chamber. Height of the water column is kept the same as the height of the fuel in actual 220t/hr CFB boiler.
2. The fan is turned on which lets the primary air at 20°C to enter the wind-box. From here, the primary air enters the combustion chamber via the nozzles. The fan speed is varied via a control box in order to carry out tests at different primary air velocities.
3. When the primary-air exits the nozzles, bubbles are formed in the combustion chamber. Visual inspections have been carried out on the size uniformity of these bubbles.
4. Measurements of air flow velocity in z-direction (towards the nozzles and the combustions chamber) are obtained on cross-sectional plane P1 (at monitoring points M21, M22 and M23) using the hot wire anemometer.
5. Air flow velocity data is analysed to quantify the effectiveness of the air modifier for air flow uniformity within the wind-box.

Table 3. Operating conditions during cold tests

Test condition	Fan's operating frequency (Hz)	Air volume (Nm ³ /hr)
1	10.7	1574.3
2	20.7	3633.1
3	30.2	6055.2
4	40.3	7871.9
5	50.0	12110.4

The visual inspection of air bubbles in the combustion chamber of the optimised CFB boiler, as shown in figure 25, helps in investigations the performance of the flow modifier. It determines the effectiveness of air flow modifier installed in the wind-box by careful observations of the air bubbles' distribution in the combustion chamber filled with water. It can be seen in figure 25 that the air bubbles are evenly distributed within the combustion chamber, and there are no localised regions of high or low concentrations of air. This implies that air flow velocity in the combustion chamber is uniform, clearly indicating the effectiveness of air flow modifier used in the optimised CFB boiler.

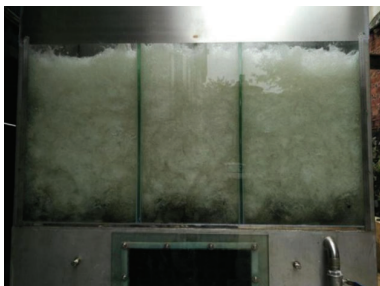


Figure 25. Visual inspection of air bubbles in the combustion chamber

Based on the measurements taken using the hot wire anemometer, figure 26 depicts the variations in the z component of air flow velocity, at different flow conditions mentioned in table 3, at the measuring points considered here (i.e. just upstream the nozzles). It can be clearly seen that as the fan speed increases, air flow velocity within the wind-box increases. Furthermore, at individual operating conditions, the z component of flow velocity remains almost the same, with a maximum variation of less than 10% observed in case of condition 5 i.e. at fan's operating frequency of 50Hz. As the fan speed decreases, these variations also decrease. These low variations in the z component of the flow velocity indicate that the flow is uniformly distributed within the wind-box of the optimised CFB boiler, and thus, the optimised flow modifier considered in the present study is substantially effective in enhancing the thermal efficiency of the boiler.

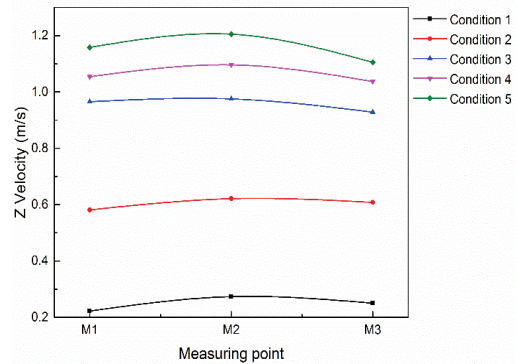


Figure 26. Variations in z component of air flow velocity on the cross-sectional plane P1 at different operating conditions

7. Application of optimally designed air flow modifier to full scale CFB boiler

The effectiveness of using the optimally designed air flow modifier has been discussed in detail, both numerically and experimentally (using cold tests) however, its effectiveness to a full scale CFB boiler yet needs to be evaluated. Thus, numerical simulations have been performed in order to quantify the effectiveness of using optimally designed air flow modifier installed in a 220t/hr CFB boiler. The necessary adjustments have been made to the flow modifier from the design point of view in order to install it in the full scale boiler model.

Figure 27 depicts the variations in the z component of flow velocity on cross-sectional plane P1, where figure 27(a) shows the boiler without the flow modifier, while figure 27(b) shows the boiler with the optimally designed flow modifier installed. It can be clearly seen in figure 27(a) that a large scale vortical structure is present just upstream the nozzles, as observed earlier in case of small scale boiler model. In figure 27(b) it can be seen that once the optimally designed air flow modifier is installed within the wind-box of the full scale CFB boiler, the vortical structures disappear, and the flow becomes significantly more uniform. This is accompanied with substantial reduction in the air flow velocity on the plane P1. It is evident from figure 27 that the installation of an air flow modifier within a 220t/hr CFB boiler enhances the thermal efficiency of the boiler by making the air flow more evenly distributed. Hence, the qualitative trends are in-line with the discussions presented earlier in the present study.

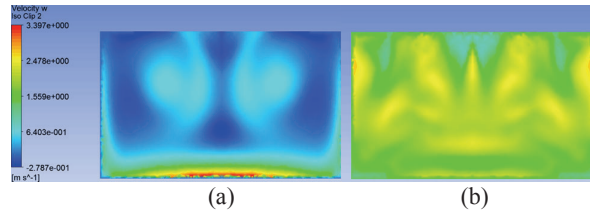


Figure 27. Variations in the z component of air flow velocity on cross-sectional plane P1 for a 220t/hr CFB boiler (a) without the flow modifier (b) installed with the optimally designed air flow modifier

Using equation (2), flow velocity inhomogeneity has been computed on the cross-sectional plane P for the two boilers considered in figure 27. The value of flow velocity inhomogeneity in case of 220t/hr CFB boiler not fitted with the flow modifier is 65.79%, which was 81% in case of its small scale model. This leads to significantly higher flow velocities of the flue gas in the combustion chamber. A number of small carbon particles remain unburned and are carried out of combustion chamber due to this. As a result, the thermal efficiency of the CFB boiler is lower than expected. The flow velocity inhomogeneity in case of 220t/hr CFB boiler installed with optimally designed flow air modifier is 21.25, which was 24% in its small scale counterpart. The low velocity inhomogeneity reduction ($\Delta\xi$) has been computed to be $(65.79-21.25)/65.79=70\%$ on cross-sectional plane P1 of 220t/hr CFB boilers considered in figure 28. $\Delta\xi$ in case of small scale CFB boiler model was also 70%, thus the effectiveness of using the optimally designed air flow modifier is established here.

7.1. Results of hot test

The final verification of the aforementioned results has been carried out by Guang Dong Special Equipment Test and Research Institute [1, 44] in their hot test reports. The results of hot test are summarised in table 4. It can be seen towards the end of the table that heat losses in the 200t/hr CFB boiler, installed

Table 4. Results of hot test

Test Items	Symbol	Unit	Before retrofit	After retrofit	% change
Carbon percentage of the received base	C_{ar}	%	43.82	42.51	-3.0
Hydrogen percentage of the received base	H_{ar}	%	2.81	2.84	1.1
Oxygen percentage of the received base	O_{ar}	%	8.09	7.67	-5.2
Nitrogen percentage of the received base	N_{ar}	%	0.8	0.32	-60.0
Sulphur percentage of the received base	S_{ar}	%	0.41	0.41	0.0
Water percentage of the received base	M_{ar}	%	19.6	19.8	1.0
Ash percentage of the received base	A_{ar}	%	24.47	24.47	0.0
Low calorific value	Q_{dw}	kJ/kg	15108	14875	-1.5
Unburned carbon content in slag	C_{dz}	%	0.91	0.65	-28.6
Percentage of slag content accounting for the total ash content	α_{dz}	%	20	20	0.0
Unburned carbon content in fly ash	C_{fh}	%	1.8	1.5	-16.7
Percentage of fly ash content accounting for the total ash content	α_{fh}	%	80	80	0.0
Exhaust flue gas temperature	θ_{py}	°C	168.5	157.1	-6.8
Oxygen content in exhaust flue gas	V_{O_2}	%	9.13	7.72	-15.4
CO content in exhaust flue gas	V_{CO}	%	0.0053	0.0048	-9.4
CO ₂ content in exhaust flue gas	V_{CO_2}	%	10.82	12.34	14.0
Exhaust flue gas heat loss	q_2	%	12.29	9.93	-19.2
Heat loss from incomplete combustion of flammable gas	q_3	%	0.04	0.03	-25.0
Heat loss from incomplete combustion of solid	q_4	%	0.9	0.64	-28.9
Heat loss from boiler radiation	q_5	%	0.85	0.4	-52.9
Heat loss from ash slag	q_6	%	0.21	0.21	0.0
Thermal efficiency of boiler	η	%	85.71	88.34	3.1

with an optimally designed air flow modifier, have significantly decreased. Hence, the thermal efficiency of the boiler has been shown to increase from 85.71% to 88.34%, which is equivalent to savings of 5,000 tons of coal per year. The economic benefits of this energy-saving technology are very significant, and hence, it confirms the effectiveness of the optimally designed air flow modifier.

7.2. Error Analysis of the thermal efficiency of the boiler

After conducting the hot test, the reliability of the boiler's thermal efficiency needs to be evaluated using error analysis approach. The detailed description regarding the principles of error analysis can be found in [45]. According to [46], the boiler's thermal efficiency can be expressed as:

$$\eta_{gl} = q_1 = 100 - \sum_{i=2}^6 q_i \quad (\%) \quad (4)$$

where q_i ($i=1, 2, 3, 4, 5$ and 6) represents net heat (q_1), heat loss due to exhaust gas (q_2), heat loss due to unburned gas (q_3), heat loss due to unburned carbon (q_4), heat loss due to radiation (q_5) and heat loss due to sensible heat in slag (q_6) respectively.

According to [47], the following empirical equations can be used to calculate the values of q_2, q_3, q_4, q_5 and q_6 :

$$q_2 = (m + n\alpha_{py}) \left(1 - \frac{q_4}{100}\right) \frac{\theta_{py} - t_{amb}}{100} \quad (\%) \quad (5)$$

where $m=0.5, n=3.45, \alpha_{py}$ is excess air coefficient, θ_{py} is exhaust gas temperature and t_{amb} is ambient temperature.

$$q_3 = \lambda\alpha_{py}V_{CO} \quad (\%) \quad (6)$$

where $\lambda=3.2$ and V_{CO} is the volume percentage of CO in exhaust flue gas.

$$q_4 = \frac{B A_{ar}}{Q_r} \left(\frac{a_{hz} C_{hz}}{100 - C_{hz}} + \frac{a_{fh} C_{fh}}{100 - C_{fh}} \right) \quad (\%) \quad (7)$$

where B is the calorific value of combustible material = 33700kJ/kg, A_{ar} is the Ash percentage of the received base in %, Q_r is the low calorific value of the received basis in kJ/kg, C_{hz} and C_{fh} represent the weight percentage of combustible material in coal slag and fly ash in % respectively, and a_{hz} and a_{fh} represent the percentage of coal slag content and fly ash content in total amount of fuel ash in % respectively. In the current study, according to [42, 44], $a_{hz}=0.2$ and $a_{fh}=0.8$.

$$q_5 = -\frac{hX}{100X_0} + d \text{ (\%)} \quad (8)$$

where $h=0.33$, $d=0.495$, X_0 and X are the rated and current loads of the boiler respectively.

$$q_6 = a_{hz} \frac{100}{100-C_{hz}} (c\theta)_{hz} \frac{A_{ar}}{Q_r} \quad (9)$$

where $(c\theta)_{hz}$ is the enthalpy of coal slag. Combining equations (4-7):

$$\eta_{gl} = 100 - \left[(m + n\alpha_{py}) \left(1 - \frac{q_4}{100} \right) \frac{\theta_{py}-t_{amb}}{100} + \lambda\alpha_{py}V_{CO} + \frac{B A_{ar}}{Q_r} \left(\frac{a_{hz} C_{hz}}{100-C_{hz}} + \frac{a_{fh} C_{fh}}{100-C_{fh}} \right) + \left(-\frac{hX}{100X_0} + d \right) + a_{hz} \frac{100}{100-C_{hz}} (c\theta)_{hz} \frac{A_{ar}}{Q_r} \right] \quad (10)$$

where [46]:

$$(c\theta)_{hz} = 0.0002887\theta_{py}^2 + 0.6851\theta_{py} + 26.76 \quad (11)$$

$$\alpha_{py} \approx \frac{0.21}{0.21-V_{O_2}} \quad (12)$$

Thus:

$$\eta_{gl} = f(\theta_{py}, V_{O_2}, V_{CO}, C_{fh}, C_{hz}, A_{ar}, Q_r) = f(X_1, X_2, X_3, X_4, X_5, X_6, X_7) \quad (13)$$

Based on the principles of calculus, the following equation can be acquired:

$$\Delta\eta_{gl} = \frac{\partial\eta_{gl}}{\partial\theta_{py}} \times \Delta\theta_{py} + \frac{\partial\eta_{gl}}{\partial V_{O_2}} \times \Delta V_{O_2} + \dots + \frac{\partial\eta_{gl}}{\partial Q_r} \times \Delta Q_r = \sum_{i=1}^7 C_i \times \Delta X_i \quad (14)$$

where $\Delta\eta_{gl}$ is the test error in the thermal efficiency of the boiler, ΔX_i is the measurement error in X_i , $C_i = \frac{\partial\eta_{gl}}{\partial X_i} = \frac{\Delta\eta_{gl}}{\Delta X_{ii}}$ where ΔX_{ii} is fractional change in X_i (0.1%) and $\Delta\eta_{gl}$ is the variation in η_{gl} caused by ΔX_{ii} [47]. The results of the error analysis for the 220t/hr CFB boiler are summarised in table 6. It can be clearly seen in table 6 that the maximum test error in the thermal efficiency of the 220t/h CFB boiler is 0.581%. Hence, the results presented in table 5 regarding the increase in the thermal efficiency of the 220t/hr CFB boiler (by 3.1%), after the installation of optimally designed air flow modifier in its wind-box, is thus confirmed.

Table 5. Results of error analysis

Items	Symbol	Unit	Value	Accuracy	ΔX_i	C_i	$C_i \times \Delta X_i$
Exhaust flue gas temperature	θ_{py}	°C	157.1	0.1°C	0.1°C	0.0587	0.006
Oxygen content in exhaust flue gas	V_{O_2}	%	7.72	0.01%	0.00077	206.3	0.159
CO content in exhaust flue gas	V_{CO}	%	0.048	1ppm	0.000001	2445.9	0.002
Unburned carbon content in fly ash	C_{fh}	%	1.5	1%	0.00015	826.8	0.124
Unburned carbon content in slag	C_{hz}	%	0.65	1%	0.000065	1813.7	0.118
Ash percentage of the received base	A_{ar}	%	24.47	0.5%	0.00122	51.13	0.063
Low calorific value	Q_r	kJ/kg	14875	1%	148.75	0.00073	0.109
Test error in the thermal efficiency	$\Delta\eta_{gl}$	%					0.581

8. Conclusions

The primary aim of the present study is to carry out numerical and experimental investigations on the flow distribution in the primary air supply system of a 220t/hr CFB boiler. Numerical simulations and cold tests of a small scale model are carried out to analyse the flow velocity and swirl strength variations in the different sections of the wind-box, both with and without using an air flow modifier. The effectiveness of the numerical modelling is verified as the results of the numerical simulations match well with the cold test results. The same methodology has been implemented to a full scale 220t/hr CFB boiler as well. The hot test results depict that the thermal efficiency of the boiler increases from 85.71% to 88.34%, and hence the effectiveness of the air flow modifier is established. Based on the analysis of the results, it can be concluded that:

(a) The results obtained from the numerical modeling of the CFB boiler exhibit that flow recirculation is predominant in the wind-box, which can be effectively eliminated by

installing an air flow modifier composed of three baffles and a perforated plate.

- (b) The uniformity of air flow in the wind-box has been significantly improved as the inhomogeneity of air flow velocity in the cross-sectional plane P1 reduces by 70%. This verifies the effectiveness of the air flow modifier.
- (c) Cold test of the model shows that air flow velocity distribution in the wind-box, installed with an optimally designed flow modifier, is uniform, and the deviation between the maximum value and the minimum value does not exceed 10%. Therefore, the effectiveness of the air flow modifier is confirmed experimentally as well.
- (d) According to the results of the hot test on a 220t/hr CFB boiler, the thermal efficiency of the boiler increases from 85.71% to 88.34% when the optimally designed air flow modifier is used. This increase in the thermal efficiency of the CFB boiler corresponds to an equivalent saving of 5,000 tons of coal per year. The economic benefits of this energy-saving technology are very significant.

Acknowledgements

This work is supported by the Scientific and Technological Plan of Guangdong Province (No. 2010B080701003) and the University of Huddersfield, United Kingdom.

References

- L. Li, (2017) Hot test report of a 220t/hr CFB boiler before retrofit, Report submitted to Guang Dong Special Equipment Test and Research Institute.
- G. Yue, R. Cai, J. Lu and H. Zhang (2017) From a CFB reactor to a CFB boiler – The review of R&D progress of CFB coal combustion technology in China, *Powder Technology* (7) 18-28.
- R. Cai and Y. Zhang (2016) Force characteristic of a large dense object in a fluidized bed equipped with an inclined air distributor, *Advanced Powder Technology* (27) 599-609.
- R. Cai, C. Gu, Y. Zhang, Q. Li and A. Meng (2015) Effect of inclined distributor on the motion behavior of a large spherical object in the bottom zone of a fluidized bed, *Powder Technology* (277) 147-155.
- F. Rahimpour, R. Zarghami and N. Mostoufi (2017) Effect of distributor on fluidized bed hydrodynamics, *Chemical Engineering* (95) 2221-2234.
- M. Wormsbecker, T. S. Pugsley and H. Tanfara (2007) The influence of distributor design on fluidized bed dryer hydrodynamics, *Proceedings of the 12th International Conference on Fluidization-New Horizons in Fluidization Engineering, Engineering Conferences International*, 13-17 May, Vancouver, Canada.
- L. Luo, M. Wei, Y. Fan and G. Flamant (2015) Heuristic shape optimization of baffled fluid distributor for uniform flow distribution, *Chemical Engineering Science* (123) 542-556.
- M. Al-Rawashdeh, X. Nijhuis, E. V. Rebrov, V. Hessel and J. C. Schouten (2012) Design methodology for barrier-based two phase flow distributor, *American Institute of Chemical Engineers Journal* (58) 3482-3493.
- M. Al-Rawashdeh, F. Yu, T. A. Nijhuis, E. V. Rebrov, V. Hessel and J. C. Schouten (2012) Numbered-up gas-liquid micro/millichannels reactor with modular flow distributor, *Chemical Engineering Journal* (207-208) 645-655.
- X. Guo, Y. Fan and L. Luo (2013) Mixing performance assessment of a multi-channel mini heat exchanger reactor with arborescent distributor and collector, *Chemical Engineering Journal* (227) 116-127.
- R. M. Kumaran, G. Kumaraguruparan and T. Sornakumar (2013) Experimental and numerical studies of header design and inlet/outlet configurations on flow maldistribution in parallel micro-channels, *Applied Thermal Engineering* (58) 205-216.
- M. Wei, Y. Fan, L. Luo and G. Flamant (2017) Design and optimization of baffled fluid distributor for realizing target flow distribution in a tubular solar receiver, *Energy* (136) 126-134.
- M. Wei, Y. Fan, L. Luo and G. Flamant (2015) CFD-based evolutionary algorithm for therealization of target fluid flow distribution among parallel channels, *Chemical Engineering Research and Design* (100) 341-352.
- C. Pistoiesi, Y. Fan and L. Luo (2015) Numerical study on the improvement of flow distribution uniformity among parallel mini-channels, *Chemical Engineering and Processing: Process Intensification* (95) 63-71.
- J. Lee, D. Kim, J. Kim, K. Park and T. Lee (2013) Evaluation of the performance of a commercial circulating fluidized bed boiler by using IEA-CFBC model: Effect of primary to secondary air ratio, *Korean Journal of Chemical Engineering* (30) 1058-1066.
- P. Mirek (2011) Designing of primary air nozzles for large-scale CFB boilers in a combined numerical-experimental approach, *Chemical Engineering and Processing* (50) 694-701.
- P. Mirek and W. Nowak (2008) The influence of air distributor's geometry on combustion conditions in large-scale CFB boiler, *Archive of Thermodynamics* (29) 37-44.
- P. Mirek, R. Sekret and W. Nowak (2007) The influence of air nozzles' shape on the NO_x emission in the large-scale 670 MWt CFB boiler, *Proceedings of the 12th International Conference on Fluidization - New Horizons in Fluidization Engineering*, 13-17 May, Vancouver, Canada.
- P. Mirek, J. Mirek and W. Nowak (2005) The experimental investigation of arrowhead nozzles operating in a 235 MWe CFB boiler, *Proceedings of the 8th International Conference on Circulated Fluidized Bed Technology*, 10-13 May, Hanzhou, China.
- C. Bhasker (2002) Simulation of air flow in the typical boiler wind-box segments, *Advances in Engineering Software* (33) 793-804.
- S. Balagurunathan (2001) Technical presentation on circulating fluidized bed combustion boilers on power plant systems and equipments, HRDC Training Course Material, Bhel, Hyderabad, India.
- P. Basu, C. Kefa and L. Jestin (2000) *Boiler and burners: Design and Theory*, Springer, New York, USA.
- Ansys 17.0 User Guide available online at <https://www.sharcnet.ca/Software/Ansys/17.0/en-us/help/flu Ug/flu Ug.html>
- H. K. Versteeg and W. Malalasekera (1995) *An Introduction to Computational Fluid Dynamics*, Longman Scientific and Technical, U.K. ISBN: 0131274988.
- C. Pozrikidis (2001) *Fluid Dynamics Theory, Computation and Numerical Simulation*, Kluwer Academic Publishers, U.S.A. ISBN: 038795869X.
- T. Asim and R. Mishra (2016) Computational Fluid Dynamics based Optimal Design of Hydraulic Capsule Pipelines Transporting Cylindrical Capsules, *International Journal of Powder Technology* (295) 180-201.
- T. Asim, R. Mishra, S. Abushaala and A. Jain (2016) Development of a Design Methodology for Hydraulic Pipelines carrying Rectangular Capsules; *International Journal of Pressure Vessels and Piping* (146) 111-128.
- T. Asim and R. Mishra (2018) Effect of capsule shape on hydrodynamic characteristics and optimal design of hydraulic capsule pipelines, *Journal of Petroleum Science and Engineering* (161) 390-408.
- T. Asim and R. Mishra (2016) Optimal Design of Hydraulic Capsule Pipelines Transporting Spherical Capsules, *The Canadian Journal of Chemical Engineering* (94) 966-979.
- T. Asim, R. Mishra, L. E. Kollar and S. R. Pradhan (2013) Optimal Sizing and Life-Cycle Cost Modelling of Pipelines Transporting Multi-Sized Solid-Liquid Mixtures, *International Journal of Pressure Vessels and Piping* (113) 40-48.
- R. Mishra, E. Palmer and J. Fieldhouse (2009) An Optimization Study of a Multiple-Row Pin-Vented Brake Disc to Promote Brake Cooling Using Computational Fluid Dynamics, *Proceedings of the Institution of Mechanical Engineers, Part D: Journal of Automobile Engineering* (223) 865-875.
- T. Asim and R. Mishra (2017) Large Eddy Simulation based Analysis of Complex Flow Structures within the Volute of a Vaneless Centrifugal Pump, *Sadhana* (42) 505-516.
- R. Mishra, S. N. Singh and V. Seshadri (1998) Velocity measurement in solid-liquid flows using an impact probe, *Flow Measurement and Instrumentation* (8) 157-165.
- B. Tesfa, F. Gu, R. Mishra and A. Ball (2013) LHV predication models and LHV effect on the performance of CI engine running with biodiesel blends, *Energy Conversion and Management* (71) 217-226.
- R. Mishra, S. N. Singh and V. Seshadri (1998) Improved model for the prediction of pressure drop and velocity field in multi-sized particulate slurry flow through horizontal pipes, *Powder Handling and Processing* (10) 279-287.
- T. Asim, R. Mishra, M. Charlton and C. Oliveira (2015) Capacity Testing and Local Flow Analysis of a Geometrically Complex Trim Installed within a Commercial Control Valve, *International Conference on Jets, Wakes and Separated Flows*, 16-18 June, Stockholm, Sweden.
- T. Asim, M. Charlton and R. Mishra (2017) CFD based Investigations for the Design of control Valves used in Energy Systems, *Energy Conversion and Management* (153) 288-303.
- M. Charlton, T. Asim and R. Mishra (2016) The effect of Manufacturing Method Induced Roughness on control Valve Performance, 6th International and 43rd National Conference on Fluid Mechanics and Fluid Power, 15-17 December, MNNIT, Allahabad, India.
- T. Asim (2013) Capacity testing of X-Stream valves for single-component single-phase flows, Technical report submitted to Weir Valves and Controls Ltd.
- A. Oliveira (2017) Capacity testing of X-Stream valves for single-component single-phase flows, Technical report submitted to Weir Valves and Controls Ltd.

40. T. Asim (2013) Computational Fluid Dynamics based Diagnostics and Optimal Design of Hydraulic Capsule Pipelines, Ph.D. Thesis, University of Huddersfield Huddersfield, U.K.
41. G. Taguchi (1986) Introduction to Quality Engineering: Designing Quality into Products and Processes, Asian Productivity Organisation, Tokyo, Japan.
42. G. Taguchi and S. Konishi (1987) Orthogonal Arrays and Linear Graphs: Tools for Quality Engineering, American Supplier Institute Press, Dearborn, U.S.A.
43. J. Zhu, Z. Ouyang and Q. Lu (2013) Numerical Simulation on Pulverized Coal Combustion and NO_x Emissions in High Temperature Air from Circulating Fluidized Bed, *Journal of Thermal Science* (22) 261-268.
44. L. Li (2017) Hot test report of a 220t/hr CFB boiler after retrofit, Guang Dong Special Equipment Test and Research Institute, Guangdong University of Technology, Guangzhou, China.
45. P. R. Bevington and D. K. Robinson (1992) Data Reduction and Error Analysis for the Physical Sciences, 3rd ed., McGraw-Hill, New York, USA.
46. J. Wu, Y. Zhang, G. Xu, Y. Lin and X. Lv (2014) Research on the Optimization of Boiler Efficiency based on Artificial Bee Colony Algorithm, *Computer and Information Science* (7) 30-38.
47. Z. Xunjia, L. Jingyan, W. Jiangwei and J. Lincan (2012) Analysis and Application of Uncertainty in Anti-Balancing Thermal Efficiency of Boilers, *Thermal Power Generation* (2) 32-36.